

Propagation of Muons and Taus at High Energies

S. Iyer Dutta¹, M. H. Reno², I. Sarcevic¹ and D. Seckel³

¹*Department of Physics, University of Arizona, Tucson, Arizona 85721*

²*Department of Physics and Astronomy, University of Iowa, Iowa City, Iowa 52242*

³*Bartol Research Institute, University of Delaware, Newark, Delaware 19716*

Abstract

The photonuclear contribution to charged lepton energy loss has been re-evaluated taking into account HERA results on real and virtual photon interactions with nucleons. With large Q^2 processes incorporated, the average muon range in rock for muon energies of 10^9 GeV is reduced by only 5% compared with the standard treatment. We have calculated the tau energy loss for energies up to 10^9 GeV taking into consideration the decay of tau. A Monte Carlo evaluation of tau survival probability and range show that at energies below $10^7 - 10^8$ GeV, depending on the material, only tau decays are important. At higher energies the tau energy losses are significant, reducing the survival probability of the tau. We show that the average range for tau is shorter than its decay length and reduces to 17 km in water for an incident tau energy of 10^9 GeV, as compared with its decay length of 49 km at that energy. In iron, the average tau range is 4.7 km for the same incident energy.

I. INTRODUCTION

Neutrino telescopes have the potential for detecting distant sources of high energy neutrinos, for example, from Active Galactic Nuclei and Gamma Ray Bursters [1]. Upward-going muons from muon neutrino conversions to muons via charged current interactions with nuclei are the main signal of muon neutrinos [2,3]. In addition, muons as well as neutrinos are produced in the atmosphere by cosmic ray interactions with air nuclei. Underground detector measurements of muon fluxes as a function of zenith angle are one way to determine the atmospheric muon flux as a function of energy. At high energies, one expects the muon flux to reflect the onset of contributions from the production of charm in the atmosphere [4]. A good understanding of the muon energy loss at high energies is an essential ingredient to the analysis of the high energy atmospheric muon flux.

Recent SuperK measurements of atmospheric neutrinos strongly suggest $\nu_\mu \rightarrow \nu_\tau$ oscillation [5] with large mixing angle of $\sin^2 2\theta > 0.84$ and a neutrino mass squared difference of $2 \times 10^{-3} \text{ eV}^2 < \Delta m^2 < 6 \times 10^{-3} \text{ eV}^2$ [6]. Assuming $\nu_\mu \rightarrow \nu_\tau$ oscillation of extragalactic neutrinos with SuperK parameters, about half of the muon neutrinos are converted to tau neutrinos on the way to the Earth. This leads to comparable fluxes of ultrahigh energy tau neutrinos and muon neutrinos at the Earth. Tau energy loss affects tau neutrino propagation

in the Earth, where tau neutrinos interact with nucleons to produce taus which subsequently decay [7]. An understanding of tau energy loss at very high energies could help with the interpretation of long tracks produced by charged particles in large underground detectors.

Future neutrino telescopes such as AMANDA, NESTOR, ANTARES and ICECUBE are aimed at detecting high energy events from extragalactic neutrino sources. The high energy behavior of muon and tau interactions with water or rock nuclei have implications for event rates and the eventual unfolding of their respective parent neutrino flux.

One way to characterize the energy loss of charged leptons is to consider the average lepton energy loss per distance traveled (X in units of g/cm^2), which can be expressed in the form

$$-\left\langle \frac{dE}{dX} \right\rangle = \alpha + \beta E \quad (1.1)$$

where E is the lepton energy, α is nearly constant, determined by the ionization energy loss, and $\beta = \sum_i \beta^i$ is weakly dependent on energy and due to radiative energy loss through bremsstrahlung, pair production and photonuclear scattering. Generically,

$$\beta^i(E) = \frac{N}{A} \int_{y_{min}}^{y_{max}} dy y \frac{d\sigma^i(y, E)}{dy} \quad (1.2)$$

where y is the fraction of lepton energy loss in the radiative interaction:

$$y = \frac{E - E'}{E} \quad (1.3)$$

for final lepton energy E' . The superscript i denotes bremsstrahlung (brem), pair production (pair) and photonuclear (nuc) processes. Avogadro's number is N and the atomic mass number of the target nucleus is A . For rock, typical values for initial muons of energy ~ 100 GeV are $\alpha \simeq 2.4 \text{ MeV}/(\text{g cm}^{-2})$ and $\beta \simeq 3 \times 10^{-6}/(\text{g cm}^{-2})$ [8].

At low energies, continuous energy loss by ionization dominates muon propagation, but at higher energies (above $\sim 10^3$ GeV), losses through pair production, bremsstrahlung and photonuclear interactions dominate. In the case of the muon, pair production is the most important mechanism, but for taus, the photonuclear process is at least as important as pair production. The high energy extrapolation of the photonuclear cross section has the largest theoretical uncertainty in the contributions to energy loss.

The experimental interest in high energy muons and taus make it useful to reanalyze the high energy photonuclear differential cross section. Bottai and Perrone [9] have reevaluated the photonuclear contributions using the HERA results for $\sigma(\gamma N)$. In this paper, we evaluate the photonuclear differential cross section using HERA results for real *and* virtual photon-nucleon scattering. Here, we use a parameterization of the measured electromagnetic structure function F_2 which agrees well with data over the full range of Q^2 : from real photon interactions with nucleons to highly virtual photon interactions with nucleons. One expects that the inclusion of the $Q^2 \gg 0$ part of the photonuclear cross section will contribute to larger muon energy losses at high energy. Indeed, this is what we find at the highest muon energies considered. We use the same expression for photonuclear interactions of taus with the correction for the different lepton mass.

In the next section and Appendix A, we outline the formulas for evaluating charged lepton energy loss, and we review the standard treatment of the photonuclear cross section

discussed by Bezrukov and Bugaev in Ref. [10]. We outline the Monte Carlo program for energy loss (and decay, for the tau). In the following section, with details in Appendix B, we describe our treatment of the photonuclear cross section using F_2 . In Section IV, we evaluate and compare our energy losses with the standard treatment in the case of muons. Section V includes β^i , range and survival probability for taus taking into consideration the decay probability. In Section VI, we summarize our results and discuss some implications of the new high energy photonuclear contributions to charged lepton energy loss.

II. CHARGED LEPTON ENERGY LOSS

A standard compilation of the energy loss parameters for muon energy loss was performed by Lohmann, Kopp and Voss (LKV) [8]. The standard formulas are reproduced in Appendix A. In evaluating the energy loss due to ionization, the Bethe-Bloch formula [11] is used with parameters listed in Table I [12]. Bremsstrahlung energy losses are computed via the differential cross section of Petrukhin and Shestakov [13]. Improvements of the bremsstrahlung calculation [14] affect the muon intensity-depth relationship by only a few percent [15] and should affect the tau energy loss even less. The pair production differential cross section is parameterized by Kokoulin and Petrukhin [16].

The standard photonuclear differential distribution used in muon energy loss calculations is by Bezrukov and Bugaev (BB) [10]. Their differential cross section is based on a generalized vector dominance model with off-diagonal contributions, and the nuclear shadowing is evaluated using an optical model. The BB parameterization of the photonuclear cross section is a function of $A^{1/3}\sigma_{\gamma N}(E)$, as exhibited in Eqs. (A10) and (A11). Our alternative to the BB differential cross section is described in detail in the next section.

For quantitative comparisons of the two approaches to photonuclear energy loss, we use a one-dimensional Monte Carlo propagation program to evaluate survival probabilities of muons and taus as a function of energy and depth X . By using the dE/dX formula and integrating, one can find the “range of average energy loss” $R_{\langle\Delta E\rangle}$. Lipari and Stanev (LS) have shown that this is different than the average range $\langle R(E)\rangle$ [17]. With a stochastic treatment of bremsstrahlung, pair production and photonuclear interactions, fluctuations have the effect of decreasing the average range relative to the range of average energy loss. Accounting for fluctuations has implications for the downward muon rates where the tails of the survival probabilities are important [17]. The Lipari-Stanev evaluation of the muon range relies on the Bezrukov-Bugaev photonuclear contribution.

The one-dimensional approximation, where the outgoing charged lepton travels in the same direction as the incident lepton, should be adequate for the high energies considered here. More elaborate (three-dimensional) evaluations have been performed by other authors, for example, in the program MUSIC by Antonioli *et al.* [15]. The MUSIC program compares well with the one-dimensional Lipari-Stanev survival probabilities, both of which use the differential cross sections outlined in LKV.

In constructing our Monte Carlo program, we follow the standard procedure of splitting the radiative energy loss into two terms, a continuous “soft” term for $y \leq y_{cut}$, and a stochastic “hard” term for $y_{cut} < y \leq 1$ in

$$-\frac{dE}{dX} = \alpha + \frac{N}{A}E \int_0^{y_{cut}} dy y \frac{d\sigma}{dy} + \frac{N}{A}E \int_{y_{cut}}^1 dy y \frac{d\sigma}{dy}, \quad (2.1)$$

while the ionization is treated continuously. We have chosen $y_{cut} = 10^{-3}$ following Ref. [15]. For taus, we have added a stochastic term for tau decay.

III. PHOTONUCLEAR CROSS SECTION USING F_2

The photonuclear cross section describes the interactions of charged leptons(l) with nuclei via virtual photon exchange. The dominant part of the cross section is from nearly real photons (negative four-momentum squared $Q^2 \rightarrow 0$), however, this is the limit where energy loss is negligible. Our approach here is to treat the $lN \rightarrow lX$ using the deep-inelastic scattering formalism, and to use a nucleon structure function F_2 consistent with data over the full range of Q^2 . In this approach, both soft physics at low Q^2 and hard perturbative physics at high Q^2 are incorporated. The inclusion of the perturbative physics at non-zero Q^2 has an effect on the very high energy behavior of β^{nuc} .

The standard variables used for $l(k)N(p) \rightarrow l(k')X$ scattering include

$$q^2 = (k - k')^2 = -Q^2 \quad (3.1)$$

$$x = \frac{Q^2}{2p \cdot q} \quad (3.2)$$

$$y = \frac{p \cdot q}{p \cdot k} . \quad (3.3)$$

The differential cross section can be written in the form [18]

$$\begin{aligned} \frac{d\sigma(x, Q^2)}{dQ^2 dx} = & \frac{4\pi\alpha^2}{Q^4} \frac{F_2(x, Q^2)}{x} \left[1 - y - \frac{Mxy}{2E} \right. \\ & \left. + \left(1 - \frac{2m_l^2}{Q^2} \right) \frac{y^2(1 + 4M^2x^2/Q^2)}{2(1 + R(x, Q^2))} \right] . \end{aligned} \quad (3.4)$$

The quantity R is written in terms of F_L and F_1 where

$$R(x, Q^2) = \frac{F_L(x, Q^2)}{2xF_1(x, Q^2)} \quad (3.5)$$

$$F_L(x, Q^2) = \left(1 + \frac{4M^2x^2}{Q^2} \right) F_2(x, Q^2) - 2xF_1(x, Q^2) . \quad (3.6)$$

In all of the expressions above, m_l is the lepton mass and M is the nucleon mass. We have converted the differential cross section to a dependence on y and Q^2 and used the following limits of integration:

$$Q_{\min}^2 \leq Q^2 \leq 2MEy - ((M + m_\pi)^2 - M^2) \quad (3.7)$$

$$y_{\min} \leq y \leq 1 - m_l/E . \quad (3.8)$$

where $Q_{\min}^2 \simeq m_l^2 y^2 / (1 - y)$ and $y_{\min} \simeq ((M + m_\pi)^2 - M^2) / (2ME)$.

The structure function $F_L(x, Q^2)$ is proportional to the longitudinal photon-nucleon cross section. In the $Q^2 \rightarrow 0$ limit, $F_L \sim Q^4$ while $F_1 \rightarrow Q^2$, so $R \rightarrow 0$. We have used $R(x, Q^2)$ modeled by Badelek, Kwieciński and Stasto in Ref. [19] for $10^{-7} < x < 0.1$ and 0.01

$\text{GeV}^2 < Q^2 < 50 \text{ GeV}^2$. For $x > 0.1$, the parameterization of Whitlow et al. [20] is used. There is no evidence for target dependence of R . The photonuclear β^{nuc} for muons evaluated with the R parameterized by Badelek *et al.* differs only by a few percent from that calculated with $R = 0$. Consequently, in what follows, we set $R = 0$.

The nuclear structure function depends on the particular target. The attenuation of quark density in a nucleus has been observed in deep inelastic lepton scattering (DIS) from nuclei at CERN [21] and Fermilab [22] energies in the region of small values of x and Q^2 . The data, taken over a wide kinematic range $10^{-5} < x < 0.1$ and $0.05 \text{ GeV}^2 < Q^2 < 100 \text{ GeV}^2$, show a systematic reduction of nuclear structure function $F_2^A(x, Q^2)/A$ with respect to the free nucleon structure function $F_2^N(x, Q^2)$. We define the shadowing ratio by

$$a(A, x, Q^2) = \frac{F_2^A(x, Q^2)}{AF_2^N(x, Q^2)}. \quad (3.9)$$

The origin of nuclear shadowing effect is coherent scattering of the virtual photon off the nucleons inside the nucleus in the small x region. The coherent multiple scattering can be most conveniently handled by the Glauber diffractive approximation model [23]. The interactions of the virtual photons with nucleons is modeled differently for high Q^2 and low Q^2 . At low Q^2 ($< 1 \text{ GeV}^2$), calculations of shadowing [24] have often used the vector-meson-dominance (VMD) model [25], in which the virtual photon interacts with the nucleons via its hadronic fluctuations, namely the ρ , ω and ϕ mesons. At higher Q^2 , the picture is instead that the virtual photon interacts with partonic components of the nucleons via its quark-antiquark pair ($q\bar{q}$) color-singlet fluctuation [26]. Given the high nucleon and parton densities, the quarks and gluons that belong to different nucleons in the nucleus will recombine and annihilate, leading to the so-called recombination effect first suggested by Gribov, Levin and Ryskin [27] and later proven by Mueller and Qiu [28]. The net effect of either mechanism is that F_2^A is lower than one would expect by naive superposition (AF_2^N) and weakly dependent on Q^2 in the range of interest for the photonuclear cross section. We take a Q^2 independent function of x and A consistent with the Fermilab E665 data taken in the kinematic range of $0.0001 < x < 0.56$ and $0.1 < Q^2 < 80 \text{ GeV}^2$ [22]:

$$a(A, x, Q^2) \simeq a(A, x) = \begin{cases} A^{-0.1} & x < 0.0014 \text{ ,} \\ A^{0.069 \log_{10} x + 0.097} & 0.0014 < x < 0.04 \text{ ,} \\ 1 & 0.04 < x \text{ .} \end{cases} \quad (3.10)$$

The structure function F_2^A is approximated by

$$\begin{aligned} F_2^A &= a(A, x) \frac{A}{2} (F_2^p + F_2^n) \\ &= a(A, x) A \frac{1}{2} (1 + P(x)) F_2^p \text{ ,} \end{aligned} \quad (3.11)$$

assuming $Z = A/2$. Here $P(x) = 1 - 1.85x + 2.45x^2 - 2.35x^3 + x^4$ describes the ratio F_2^n/F_2^p , parameterized by the BCDMS experiment [29].

The quantity $F_2^p(x, Q^2)$ is extracted in a variety of experiments in a range of $0 < Q^2 < 5000 \text{ GeV}^2$ and $5 \times 10^{-6} < x < 1$, though kinematic limits restrict the range of Q^2 and x in a given experiment. The differential cross section must be integrated from $Q^2 = 0$, where the perturbative QCD description of F_2 is not valid, to values of Q^2 where QCD is

valid. Consequently, a parameterization of F_2^p consistent with all the data is most useful for our purposes. The parameterization of F_2^p used here is the one by Abramowicz, Levin, Levy and Maor (ALLM) [30]. The ALLM parameterization involves two terms: a pomeron contribution and a reggeon contribution. Parameters are used to fit all data available from the pre-HERA era as well as H1 and ZEUS data published through 1997. The specific form with parameters is detailed in the Appendix B.

Eq. (3.4) shows the alternative to the BB formula for $d\sigma/dy$ which appears in Appendix A. As an initial comparison of the two approaches, we show in Fig. 1 the cross section for real photon-nucleon scattering, as a function of incident photon energy,

$$\sigma(\gamma N) = \lim_{Q^2 \rightarrow 0} \frac{4\pi^2 \alpha F_2^N}{Q^2} \quad (3.12)$$

indicated by the solid line, and the Bezrukov-Bugaev cross section (dashed line). Photon-proton data collected in Ref. [31] are also shown. Our cross section agrees with the BB parameterization at energies below $E_\gamma \sim 10^4$ GeV, however the BB cross section increases more quickly with energy. At $E_\gamma = 10^9$ GeV, our cross section is 0.40 mb, while the BB cross section is 0.58 mb.

For the calculation of the lepton propagation in rock, it is useful to compare the γA cross section for standard rock ($A = 22$). Here we include the nuclear shadowing effects. Our results are shown in Fig. 2 with the solid line. The BB cross section is the dashed line. We note that our results are in agreement with the BB parameterization for γA , namely

$$\sigma(\gamma A) = A\sigma(\gamma N)[0.75G(x) + 0.25] , \quad (3.13)$$

where x , $G(x)$ and $\sigma(\gamma N)$ appear in Eq. (A11), over a wide energy. The largest deviation occurs at the lowest photon energy shown, where the photo-nuclear contribution is least important for charged lepton energy loss.

IV. MUON ENERGY LOSS, SURVIVAL PROBABILITY, AND RANGE

The expected average muon energy loss in traversing a material of depth ΔX is characterized by $\langle dE/dX \rangle$, indicated in Eq. (1.1). The results for the standard bremsstrahlung, pair production and photonuclear (BB) differential cross sections summarized by LKV, and our results of using the ALLM differential cross section are shown in Fig. 3. Our result for β^{nuc} begins to diverge from the standard values at $E \sim 10^6$ GeV, and is a factor of about 1.6 higher at $E = 10^9$ GeV. In terms of the total β , the total with ALLM contributions is a factor of 1.15 larger than with the BB photonuclear contribution at $E = 10^9$ GeV.

To explore the effect of the slightly larger value of β^{nuc} for muons, we have evaluated the muon survival probability in standard rock. The survival probability $P(E, X)$ for a muon to survive to a depth X given incident energy E incorporates the effects of fluctuations due to radiation. In Fig. 4, we show our muon survival probabilities (solid lines) for $E = 10^3 - 10^9$ GeV, in decades of energy, versus survival depth X (in km.w.e.) for standard rock ($A = 22$ and $\rho = 2.65$ g/cm³). We have taken $E_{\text{min}} = 1$ GeV in the Monte Carlo. Using the LKV defaults in our Monte Carlo program yields the dashed lines, which agree with the Lipari-Stanev result in Ref. [17].

The two sets of survival probabilities translate to average muon ranges with incident energy E and final energy $E_{min} = 1$ GeV. The average range $\langle R(E) \rangle$ is defined by

$$\langle R(E) \rangle = \int_0^\infty dX P(E, X) . \quad (4.1)$$

The average ranges for our calculation are shown in Fig. 5 by the solid lines. The standard LKV ranges that we have calculated using the same muon transport Monte Carlo simulation are shown with dashed lines. At $E = 10^9$ GeV, the two calculations differ by only 5%. The deviation from the standard calculation increases with energy.

V. TAU ENERGY LOSS, SURVIVAL PROBABILITY, AND RANGE

Essentially the same procedure for calculating muon energy loss can be applied to the tau lepton, with the important modification that the tau has a decay length considerably shorter than the muon decay length. We have evaluated the pair production, bremsstrahlung and ionization energy loss according to the formulas in Appendix A for tau leptons, and we have evaluated the tau photonuclear differential cross section using the ALLM expression in Eq. (3.4). Fig. 6 shows the tau energy loss contributions to β for standard rock. In this figure, β is plotted on a logarithmic scale because the bremsstrahlung is very suppressed relative to the other contributions, due to the much heavier lepton mass. The photonuclear contribution to β dominates above $E \sim 10^5$ GeV.

In the absence of energy loss, the tau survival probability corresponding to the curves in Fig. 4 are exponentials of the form:

$$P(E, X) = \exp \left[-\frac{X}{\gamma c\tau\rho} \right], \quad (5.1)$$

where $\gamma = E/m_\tau$ is the Lorentz gamma factor, $c\tau = 86.93 \mu\text{m}$ is the tau decay length and ρ is the material density. The average range with no energy loss, as defined by Eq. (4.1), is just

$$\langle R(E) \rangle_{decay} = \gamma c\tau\rho . \quad (5.2)$$

For incident energies between 10^3 GeV and 10^9 GeV, we have made a Monte Carlo evaluation of tau energy loss in water, rock and iron including the electromagnetic energy loss mechanisms as described in the Appendix.

At low energies, the decay length of the tau is short and energy loss is relatively unimportant, so the survival probability is just the exponential in Eq. (5.1). The survival probability is increased at fixed depth as the energy of the tau increases. The survival probability curves can be put on the same plot by using $P(E, X)$ versus X/E as shown in Fig. 7 for water. In Fig. 7, the decay distribution Eq. (5.1) is indicated by a dashed line. A solid line overlays it, which is the probability distribution, as computed by our Monte Carlo, with incoming tau energy $E = 10^3$ GeV. The lower solid line is the survival probability for incident tau energy $E = 10^9$ GeV. The probabilities are evaluated with a minimum tau energy of 50 GeV. By changing the minimum energy to 100 GeV, we see no change in the probability distributions for incident tau energies $E = 10^3 - 10^9$ GeV.

In Fig. 8, we compare the tau decay length with the range of tau with incident energy E and final energy $E_{min} = 50$ GeV. The dashed line shows the tau decay length (Eq. (5.2)), while the solid line shows the evaluation of Eq. (4.1) including electromagnetic energy loss for propagation in water. The deviation from the simple gamma factor scaled decay length starts at about 10^8 GeV in water, and by 10^9 GeV, the average range is 35% lower. The dot-dashed and dotted lines in Fig. 8 show the tau ranges in standard rock and iron. For tau propagation in iron, the tau range is an order of magnitude shorter than its decay length for an incident energy of 10^9 GeV.

Our results differ from the estimate of the range by Fargion in Ref. [32], mainly because of the inclusion of the photonuclear and pair production processes in electromagnetic energy loss. The estimate in Ref. [32] relies on an approximate solution to Eq. (1.1), where α and β are assumed to be energy independent, and β is approximated numerically by rescaling the muon pair production β . The resulting β is more than an order of magnitude smaller than the β values we obtain, for example, in Fig. 6 for rock. As a consequence, whereas in Ref. [32], electromagnetic energy loss is never relevant, we have shown that accounting for photonuclear, bremsstrahlung and pair production energy loss mechanisms reduces the tau range in water beginning at $E \sim 10^8$ GeV, at even lower energies for more dense materials.

VI. DISCUSSION

We have re-evaluated the muon energy loss due to photonuclear interactions using the recent HERA results for the real and virtual photon-nucleon scattering. We have used the ALLM parameterization of the electromagnetic structure function $F_2(x, Q^2)$ to evaluate the photonuclear cross section including the $Q^2 \gg 0$ region. As compared with the previous Bezrukov and Bugaev result, our approach yields a change in β for photonuclear interactions.

In our evaluation of energy loss and effective ranges, except for tau decays, we have ignored the effects of weak interactions on the propagation of muons and taus. To set the scale for charged lepton energy loss via weak interactions,

$$\beta_{weak} \simeq N_A \langle y \rangle \sigma_{lN}(E) .$$

For $\langle y \rangle \simeq 0.2$ and using $\sigma_{lN} \sim \sigma_{\nu N}$ from Ref. [3], we find that for β_{weak} to be larger than a typical high energy electromagnetic $\beta \simeq 10^{-6}$ cm²/g, the charged lepton energy must be larger than $\sim 10^{16}$ GeV. Below that energy, weak interactions do not play a significant role in charged lepton energy loss.

Apart from energy loss, weak interactions also contribute to charged lepton disappearance through charged-current interactions. The tau charged-current interaction length is comparable to its decay length at energies above 10^{10} GeV in water. We have shown in Fig. 8 that already at 10^8 GeV, taus lose energy in water due to electromagnetic interactions. For tau energies above 10^{10} GeV in water, it will be an interplay of electromagnetic energy loss, decay and charged-current weak interaction disappearance of taus that will dictate tau effective ranges. Even in lead, which has a density of 11.35 g/cm³, the decay length is shorter than the charged-current interaction length for energies below a few times 10^9 GeV, so our neglect of weak interactions below $E = 10^9$ GeV is a good approximation.

The results presented here are not significantly modified by the Landau-Pomeranchuk-Migdal (LPM) effect [33]. The LPM effect arises from low-momentum transfer lepton scattering, where bremsstrahlung should, in principle, be evaluated including coherence effects due to scattering in the medium. The effect has been measured in the case of electron scattering [34] and summarized in Ref. [35], but is suppressed for heavier leptons. The suppression factor can be written crudely in terms of the photon energy $q^0 = y \cdot E$ as [35]

$$S(y, E) = \sqrt{\frac{y}{1-y} \frac{E_{LPM}}{E}} \quad (6.1)$$

when the argument of the square root is positive ($y < E/(E + E_{LPM})$), where

$$E_{LPM} = 1.38 \times 10^{13} \frac{\text{GeV}}{\text{cm}} \cdot X_0 . \quad (6.2)$$

The radiation length X_0 is 36.1 cm for water and 10.0 cm for rock. For the lepton energies of interest here, $E < 10^9$ GeV, this means that LPM suppression for muons occurs for $y < 7 \times 10^{-5}(\text{cm}/X_0)$. In practice, this affects the continuous “soft” term in Eq. (2.1). The approximation for $S(y, E)$ leads to a decrease in the soft term by at most 0.1% at the highest energies considered here. This is consistent with, for example, the more detailed evaluation of β^{brem} by Polityko *et al.* in Ref. [36], where deviations from standard β^{brem} evaluations occur above $E = 10^{11}$ GeV. The LPM effect is even further suppressed for taus, since E_{LPM} scales like the lepton mass to the fourth power.

The change to β from using the ALLM photonuclear interaction cross section increases with energy and reaches 60% for $E = 10^9$ GeV for muons. Still, for muons, the photonuclear processes do not dominate β for $E < 10^9$ GeV, and the overall effect on dE/dX is smaller. The muon survival probabilities and average muon ranges are obtained from the one dimensional Monte Carlo approximation. We find our results to be within 5% from the standard LKV value with incident energy $E < 10^9$ GeV and final energy $E_{min} = 1$ GeV.

We have evaluated the tau energy loss including the photonuclear processes as well as the ionization, pair production and bremsstrahlung energy loss. At energies above $\sim 10^8$ GeV, tau interactions become important in water and the range becomes significantly shorter. The effect appears at lower energies for more dense materials, for example, at tau energies less than 10^7 GeV for iron. We thus expect a decrease in the observed tau flux and tau neutrino energy relative to that expected if these effects had been ignored. The effect is most important for high energy taus arriving from directions just below the horizon. For directions subtending a significant portion of the Earth, energies will be degraded to less than 10^6 GeV by repeated neutrino conversion to tau and tau decay. The last few steps in that process will occur at energies where dE/dX is not important. Near the horizon, the interaction length for charged current conversion becomes comparable to the length of the chord through the Earth, and the produced taus may arrive directly in the detector depending on their range. For $E > 10^8$ GeV, the tau range is decreased in water and such taus will either not arrive or arrive at lower energies. Correspondingly, for taus produced in a detector, measured dE/dX would be higher than expected without the revised photonuclear effects calculated here.

ACKNOWLEDGMENTS

Work supported in part by National Science Foundation Grant No. PHY-9802403 and DOE Contract DE-FG02-95ER40906. We thank the Aspen Center for Physics for its hospitality while this was initiated, and we thank A. Stasto for providing us with a computer program to evaluate $R(x, Q^2)$. We acknowledge early conversations with R. Engel about using F_2 in the photonuclear process.

APPENDIX A: ENERGY LOSS FORMULAS

For completeness, we reproduce the standard formulas for ionization, pair production and bremsstrahlung energy loss. These are also collected in the unpublished work of Lohmann, Kopp and Voss [8]. The Bezrukov and Bugaev (BB) parameterization of photonuclear energy loss is also included below.

The constants are defined as follows:

$$\begin{aligned}
 \alpha &= 1/137 & (A1) \\
 N_A &= 6.023 \times 10^{23}, \text{ Avogadro's number} \\
 Z &= \text{atomic number, } A = \text{atomic weight of medium} \\
 m_e, m_l &\text{ rest masses of electron and muon or tau} \\
 \lambda_e &= 3.8616 \times 10^{-11} \text{ cm, Compton wavelength of the electron} \\
 e &= 2.718
 \end{aligned}$$

To account for energy loss on atomic electrons, the factor Z^2 in the bremsstrahlung and pair production formulas below should be replaced by $Z(Z + 1)$.

1. Ionization Energy Loss

The ionization loss for a incident muon or tau of energy E and momentum p is given by the Bethe-Bloch formula [11]:

$$\frac{dE}{dX} = \alpha^2 2\pi N_A \lambda_e^2 \frac{Z m_e}{A \beta^2} \left(\ln \frac{2m_e \beta^2 \gamma^2 E'_m}{I^2(Z)} - 2\beta^2 + \frac{E'_m{}^2}{4E^2} - \delta(X) \right) \quad (A2)$$

where

$$\begin{aligned}
 \beta &= p/E, \\
 \gamma &= E/m_l.
 \end{aligned}$$

The quantity

$$E'_m = 2m_e \frac{p^2}{m_e^2 + m_l^2 + 2m_e E} \quad (A3)$$

is the maximum energy that can be transferred to the electron. A density correction is parameterized by $\delta(X)$ for $X = \log_{10}(\beta\gamma)$ by Sternheimer *et al.* [12] as

$$\begin{aligned}
 \delta(X) &= 4.6052X + a(X_1 - X)^m + C & X_0 < X < X_1 \\
 \delta(X) &= 4.6052X + C & X > X_1.
 \end{aligned} \quad (A4)$$

The values of X_0 , X_1 , a , m , C and the mean ionization potential $I(Z)$, for rock and water are given in Table 2.

2. Bremsstrahlung Energy Loss

Following Petrukhin and Shestakov's evaluation of the form factors in the Bethe-Heitler bremsstrahlung differential cross section [13], the differential cross section used here is:

$$\frac{d\sigma}{dy} = \alpha^3 \left(2Z\lambda_e \frac{m_e}{m_l} \right)^2 \frac{1}{y} \left(\frac{4}{3} - \frac{4}{3}y + y^2 \right) \phi(\delta) , \quad (\text{A5})$$

where

$$\begin{aligned} \phi(\delta) &= \ln \left[\frac{\frac{189m_l}{m_e} Z^{-1/3}}{1 + \frac{189\sqrt{e}}{m_e} \delta Z^{-1/3}} \right], & Z \leq 10 \\ \phi(\delta) &= \ln \left[\frac{\frac{2}{3} \frac{189m_l}{m_e} Z^{-2/3}}{1 + \frac{189\sqrt{e}}{m_e} \delta Z^{-1/3}} \right], & Z > 10 \\ \delta &= \frac{m_l^2 y}{2E(1-y)} . \end{aligned} \quad (\text{A6})$$

The range of y integration is

$$0 \leq y \leq 1 - \frac{3m_l}{4E} \sqrt{e} Z^{1/3} . \quad (\text{A7})$$

3. Pair Production Energy Loss

Pair production energy loss depends on the asymmetry parameter ρ given as

$$\rho = \frac{E^+ - E^-}{E^+ + E^-}, 0 \leq |\rho| \leq \left(1 - \frac{6m_l^2}{E^2(1-y)} \right) \sqrt{1 - \frac{4m_e}{Ey}} \quad (\text{A8})$$

given E^+ and E^- , the energies of the positron and electron pair. The differential cross section is parameterized by [16]

$$\frac{d^2\sigma}{dyd\rho} = \alpha^4 \frac{2}{3\pi} (Z\lambda_e)^2 \frac{1-y}{y} \left(\phi_e + \frac{m_e^2}{m_l^2} \phi_l \right) . \quad (\text{A9})$$

where the functions ϕ_e and ϕ_l are as follows:

$$\begin{aligned} \phi_e &= \left[\left((2 + \rho^2)(1 + \beta) + \xi(3 + \rho^2) \right) \ln\left(1 + \frac{1}{\xi}\right) + \frac{1 - \rho^2 - \beta}{1 + \xi} - (3 + \rho^2) \right] L_e \\ \phi_l &= \left[\left((1 + \rho^2)(1 + \frac{3}{2}\beta) - \frac{1}{\xi}(1 + 2\beta)(1 - \rho^2) \right) \ln(1 + \xi) \right. \\ &\quad \left. + \frac{\xi(1 - \rho^2 - \beta)}{1 + \xi} + (1 + 2\beta)(1 - \rho^2) \right] L_l \\ L_e &= \ln \frac{RZ^{-\frac{1}{3}} \sqrt{(1 + \xi)(1 + Y_e)}}{1 + \frac{2m_e \sqrt{e} R Z^{-\frac{1}{3}} (1 + \xi)(1 + Y_e)}{Ey(1 - \rho^2)}} - \frac{1}{2} \ln \left[1 + \left(\frac{3m_e}{2m_l} Z^{\frac{1}{3}} \right)^2 (1 + \xi)(1 + Y_e) \right] \end{aligned} \quad (\text{A10})$$

$$\begin{aligned}
L_l &= \ln \frac{RZ^{-\frac{2}{3}} \frac{2}{3} \frac{m_l}{m_e}}{1 + \frac{2m_e \sqrt{e} R Z^{-\frac{1}{3}} (1+\xi)(1+Y_l)}{Ey(1-\rho^2)}} \\
Y_e &= \frac{5 - \rho^2 + 4\beta(1 + \rho^2)}{2(1 + 3\beta) \ln(3 + \frac{1}{\xi}) - \rho^2 - 2\beta(2 - \rho^2)} \\
Y_l &= \frac{4 + \rho^2 + 3\beta(1 + \rho^2)}{(1 + \rho^2)(\frac{3}{2} + 2\beta) \ln(3 + \xi) + 1 - \frac{3}{2}\rho^2} \\
\beta &= \frac{y^2}{2(1 - y)}, \quad \xi = \left(\frac{m_l y}{2m_e} \right)^2 \frac{(1 - \rho^2)}{(1 - y)}.
\end{aligned}$$

The value of R is $R = 189$. The range of y integration is

$$\frac{4m_e}{E} \leq y \leq 1 - \frac{3m_l}{4E} \sqrt{e} Z^{1/3}. \quad (\text{A11})$$

4. Bezrukov and Bugaev Photonuclear Energy Loss

The parameterization of the Bezrukov and Bugaev photonuclear energy loss is [10]

$$\begin{aligned}
\frac{d\sigma}{dy} &= \frac{\alpha}{2\pi} A \sigma_{\gamma N} y \left[\frac{3}{4} G(x) \left(\kappa \ln(1 + \frac{m_1}{t}) - \frac{\kappa m_1^2}{m_1^2 + t} - \frac{2m_l^2}{t} \right) + \right. \\
&\left. \frac{1}{4} \left(\kappa \ln(1 + \frac{m_2}{t}) - \frac{2m_l^2}{t} \right) + \frac{m_l^2}{2t} \left(\frac{3}{4} G(x) \frac{m_1^2}{m_1^2 + t} + \frac{1}{4} \frac{m_2^2}{t} \ln(1 + \frac{t}{m_2^2}) \right) \right]
\end{aligned} \quad (\text{A12})$$

where

$$\begin{aligned}
G(x) &= \frac{3}{x^3} \left(\frac{x^2}{2} - 1 + e^{-x}(1+x) \right) \\
x &= 0.00282 A^{\frac{1}{3}} (\sigma_{\gamma N}(E/\text{GeV})/\mu\text{b}) \\
\sigma_{\gamma N}(E) &= 114.3 + 1.647 \ln^2(0.0213 E/\text{GeV}) \mu\text{b} \\
t &= \frac{m_l^2 y^2}{(1-y)} \\
\kappa &= 1 - \frac{2}{y} + \frac{2}{y^2} \\
m_1^2 &= 0.54 \text{ GeV}^2 \\
m_2^2 &= 1.8 \text{ GeV}^2
\end{aligned} \quad (\text{A13})$$

APPENDIX B: ALLM PARAMETERIZATION OF F_2

The ALLM phenomenological parameterization of $F_2^p(x, Q^2)$ has a pomeron and reggeon contribution [30]:

$$F_2^p(x, Q^2) = \frac{Q^2}{Q^2 + m_0^2} (F_2^{\mathcal{P}}(x, Q^2) + F_2^{\mathcal{R}}(x, Q^2)) , \quad (\text{B1})$$

where the two terms have the form

$$F_2^{\mathcal{P}}(x, Q^2) = c_{\mathcal{P}}(t) x_{\mathcal{P}}^{a_{\mathcal{P}}(t)} (1-x)^{b_{\mathcal{P}}(t)} \quad (\text{B2})$$

$$F_2^{\mathcal{R}}(x, Q^2) = c_{\mathcal{R}}(t) x_{\mathcal{R}}^{a_{\mathcal{R}}(t)} (1-x)^{b_{\mathcal{R}}(t)} . \quad (\text{B3})$$

The functions $c_{\mathcal{P}}(t)$, etc., are parameterized in terms of

$$t = \ln \left(\frac{\ln(Q^2 + Q_0^2)/\Lambda^2}{\ln Q_0^2/\Lambda^2} \right) . \quad (\text{B4})$$

The form for $f = c_{\mathcal{R}}$ and $a_{\mathcal{R}}$ is

$$f = f_1 + f_2 t^{f_3} , \quad (\text{B5})$$

for $g = c_{\mathcal{P}}$ and $a_{\mathcal{P}}$,

$$g = g_1 + (g_1 - g_2) \left[\frac{1}{1 + t^{g_3}} - 1 \right] , \quad (\text{B6})$$

and finally, $h = b_{\mathcal{R}}$ and $b_{\mathcal{P}}$,

$$h = h_1^2 + h_2^2 t^{h_3} . \quad (\text{B7})$$

In the expressions for $F_2^{\mathcal{P}}$ and $F_2^{\mathcal{R}}$,

$$x_{\mathcal{P}} = \frac{Q^2 + m_{\mathcal{P}}^2}{Q^2 + m_{\mathcal{P}}^2 + W^2 - M^2} \quad (\text{B8})$$

$$x_{\mathcal{R}} = \frac{Q^2 + m_{\mathcal{R}}^2}{Q^2 + m_{\mathcal{R}}^2 + W^2 - M^2} . \quad (\text{B9})$$

The parameters satisfying the fits described in Ref. [30] are shown in Table II.

TABLES

TABLE I. Parameter values in ionization energy loss [12].

Material	I/eV	-C	X_0	X_1	a	m	Z	A	$\rho/(g/cm^3)$
Water	75.0	3.502	0.240	2.800	0.091	3.477	6.6	11.89	1.00
Standard Rock	136.4	3.774	0.049	3.055	0.083	3.412	11	22	2.65
Iron	286.0	4.291	-0.0012	3.153	0.147	2.963	26	55.84	7.87

TABLE II. Parameter values for ALLM parameterization of $F_2^p(x, Q^2)$.

$c_{\mathcal{P}1}$	0.28067	$c_{\mathcal{R}1}$	0.80107
$c_{\mathcal{P}2}$	0.22291	$c_{\mathcal{R}2}$	0.97307
$c_{\mathcal{P}3}$	2.1979	$c_{\mathcal{R}3}$	3.4942
$a_{\mathcal{P}1}$	-0.0808	$a_{\mathcal{R}1}$	0.58400
$a_{\mathcal{P}2}$	-0.44812	$a_{\mathcal{R}2}$	0.37888
$a_{\mathcal{P}3}$	1.1709	$a_{\mathcal{R}3}$	2.6063
$b_{\mathcal{P}1}$	0.60243	$b_{\mathcal{R}1}$	0.10711
$b_{\mathcal{P}2}$	1.3754	$b_{\mathcal{R}2}$	1.9386
$b_{\mathcal{P}3}$	1.8439	$b_{\mathcal{R}3}$	0.49338
$m_0^2(\text{GeV}^2)$	0.31985	$m_{\mathcal{P}}^2(\text{GeV}^2)$	49.457
$m_{\mathcal{R}}^2(\text{GeV}^2)$	0.15052	$Q_0^2(\text{GeV}^2)$	0.46017
$\Lambda^2(\text{GeV}^2)$	0.06527		

REFERENCES

- [1] See, for example, T. K. Gaisser, F. Halzen and T. Stanev, Phys. Rept. 258, 173 (1995), Erratum-ibid. 271, 355 (1996).
- [2] See, for example, R. Gandhi, C. Quigg, M. H. Reno and I. Sarcevic, Astropart. Phys. 5, 81 (1996) and references therein.
- [3] R. Gandhi, C. Quigg, M. H. Reno and I. Sarcevic, Phys. Rev. D58, 093009 (1998).
- [4] Recent evaluations of the prompt lepton flux include M. Thunman, G. Ingelman and P. Gondolo, Astropart. Phys. 5, 309 (1996); L. Pasquali, M. H. Reno and I. Sarcevic, Phys. Rev. D59, 034020 (1999); G. Gelmini, P. Gondolo and G. Varieschi, Phys. Rev. D61, 036006 (2000); G. Gelmini, P. Gondolo and G. Varieschi, Phys. Rev. D61, 056011 (2000).
- [5] S. Fukuda *et al.* (SuperKamiokande Collaboration), hep-ex/0009001.
- [6] S. Fukuda *et al.* (SuperKamiokande Collaboration), Phys. Rev. Lett. 81, 1562 (1998).
- [7] F. Halzen and D. Saltzberg, Phys. Rev. Lett. 81, 4305 (1998); for detailed evaluations for specific fluxes, see, *e.g.*, S. I. Dutta, M. H. Reno, I. Sarcevic, Phys. Rev. D62, 123001 (2000); Phys. Rev. D61, 053003 (2000) and F. Becattini and S. Bottai, astro-ph/0003179.
- [8] W. Lohmann, R. Kopp and R. Voss, CERN Yellow Report No. EP/85-03.
- [9] S. Bottai and L. Perrone, hep-ex/0001018.
- [10] L. B. Bezrukov and E. V. Bugaev, Sov. J. Nucl. Phys. 33, 635 (1981).
- [11] See, *e.g.*, B. Rossi, High Energy Particles (Prentice Hall, Englewood Cliffs, NJ, 1952).
- [12] R. M. Sternheimer *et al.*, At. Data Nucl. Data Tables 30, 261 (1984).
- [13] A. A. Petrukhin and V. V. Shestakov, Can. J. Phys. 46, S377 (1968).
- [14] S. R. Kelner, R. P. Kokoulin and A. A. Petrukhin, Phys. Atom. Nucl. 60, 576 (1997).
- [15] P. Antonioli, C. Ghetti, E. V. Korolkova, V. A. Kudryavtsev, G. Sartorelli, Astropart. Phys. 7, 357 (1997).
- [16] R. P. Kokoulin and A. A. Petrukhin, in Proceedings of the XII International Conference on Cosmic Rays (Hobart, Tasmania, Australia, 1971). Vol 6.
- [17] P. Lipari and T. Stanev, Phys. Rev. D44, 3543 (1991).
- [18] B. Badelek and J. Kwieciński, Rev. Mod. Phys. 68, 445 (1996).
- [19] B. Badelek, J. Kwieciński and A. Staśto, Z. Phys. C 74, 297 (1997).
- [20] L. W. Whitlow *et al.*, Phys. Lett. B250, 193 (1990).
- [21] NMC Collaboration, P. Amaudruz *et al.*, Z. Phys. C51, 387 (1991); Z. Phys. C53, 73 (1992); Phys. Lett. B 295, 195 (1992); NMC Collaboration, M. Arneodo *et al.*, Nucl. Phys. B 441, 12 (1995).
- [22] E665 Collaboration, M.R. Adams *et al.*, Phys. Rev. Lett. 68, 3266 (1992); Phys. Lett. B 287, 375 (1992); Z. Phys. C 67, 403 (1995).
- [23] R.J. Glauber, in *Lectures in theoretical physics*, ed. W.E. Brittin *et al.* (Interscience Publishers, New York, 1959); R.J. Glauber and G. Matthiae, Nucl. Phys. B 21, 135 (1970).
- [24] S.J. Brodsky and H.J. Lu Phys. Rev. Lett. 64, 1342 (1990).
- [25] see *e.g.*, G. Piller, W. Ratzka and W. Weise, Z. Phys. A 352, 427 (1995); T.H. Bauer, R.D. Spital and D.R. Yennie and F.M. Pipkin, Rev. Mod. Phys. 50, 261 (1978).
- [26] Z. Huang, H.J. Lu and I. Sarcevic Nucl. Phys. A 637, 79 (1998).
- [27] L.V. Gribov, E.M. Levin and M.G. Ryskin, Phys. Rep. 100, 1 (1983); E. Laenen and E. Levin, Nucl. Phys. B 451, 207 (1995).

- [28] A.H. Mueller and J. Qiu, Nucl. Phys. B 268, 427 (1986); J. Qiu, Nucl. Phys. B 291, 746 (1987).
- [29] A. C. Benvenuti et al. (BCDMS Collaboration), Phys. Lett. B237, 599 (1990).
- [30] H. Abramowicz and A. Levy, hep-ph/9712415.
- [31] C. Caso et al., Euro. Phys. J. C3, 1 (1998).
- [32] D. Fargion, astro-ph/9704205.
- [33] L. Landau and I. J. Pomeranchuk, Dokl. Akad. Nauk. SSSR 92, 535 (1953); 92, 735; A. B. Migdal, Phys. Rev. 103, 1811 (1956); Zh. Eksp. Teor. Fiz. 32, 633 (1957) (Sov. Phys. JETP 5, 527).
- [34] P. Anthony *et al.*, Phys. Rev. Lett. 75, 1949 (1995).
- [35] S. Klein, Rev. Mod. Phys. 71, 1501 (1999) and references therein.
- [36] S. Polityko, N. Takahashi, M. Kato, Y. Yamada and A. Misaki, hep-ph/9911330.

FIGURES

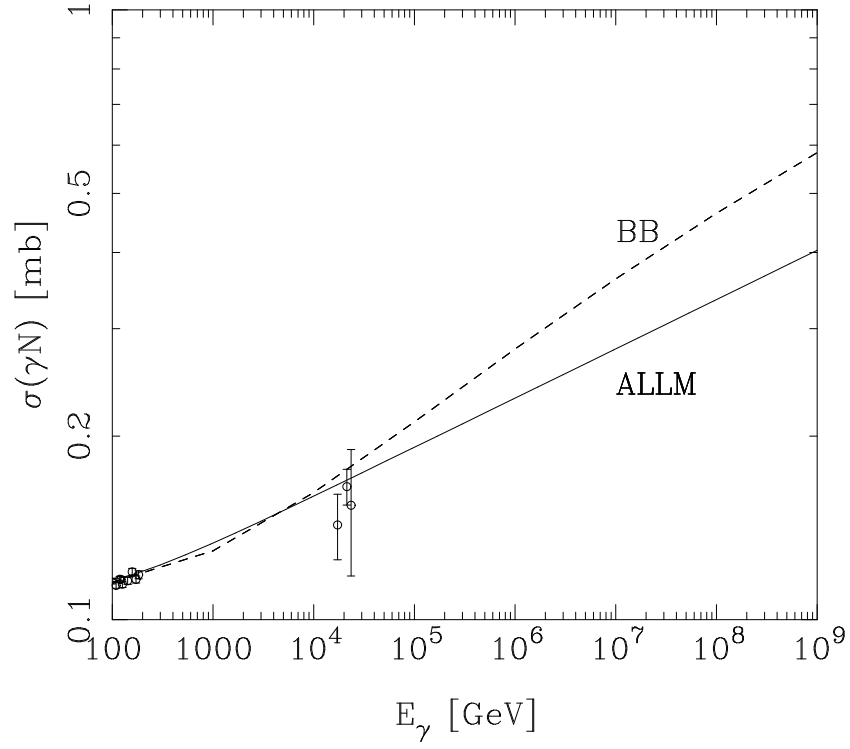


FIG. 1. The photon-nucleon cross section as a function of incident photon energy for the BB (dashed) and ALLM (solid) parameterizations. Also shown are photon-proton data collected in Ref. [30].

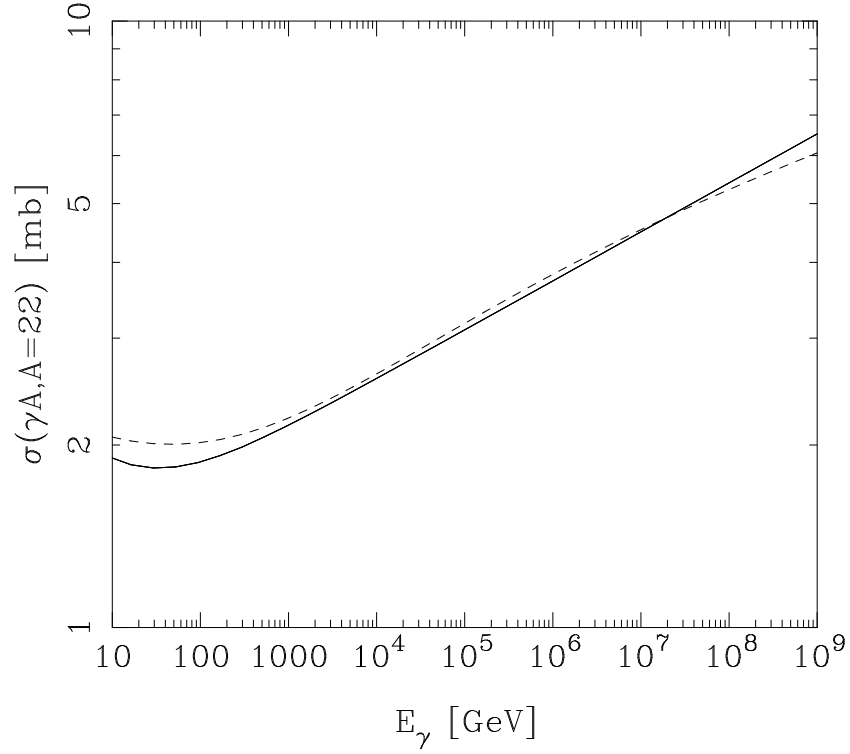


FIG. 2. The photon-nucleus cross section standard rock ($A = 22$), as a function of incident photon energy E using the ALLM parameterization and Eqs. (3.9) and (3.10) for the shadow factor and conversion to nucleon structure function.

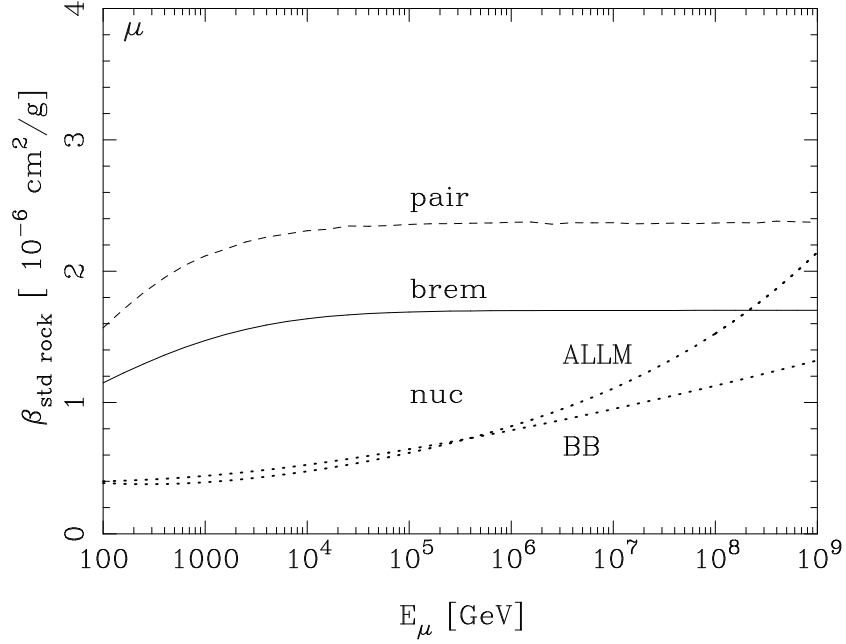


FIG. 3. The β value for muon in standard rock ($A = 22$), including bremsstrahlung (solid line), pair production (dashed) and photonuclear (dotted) interactions.

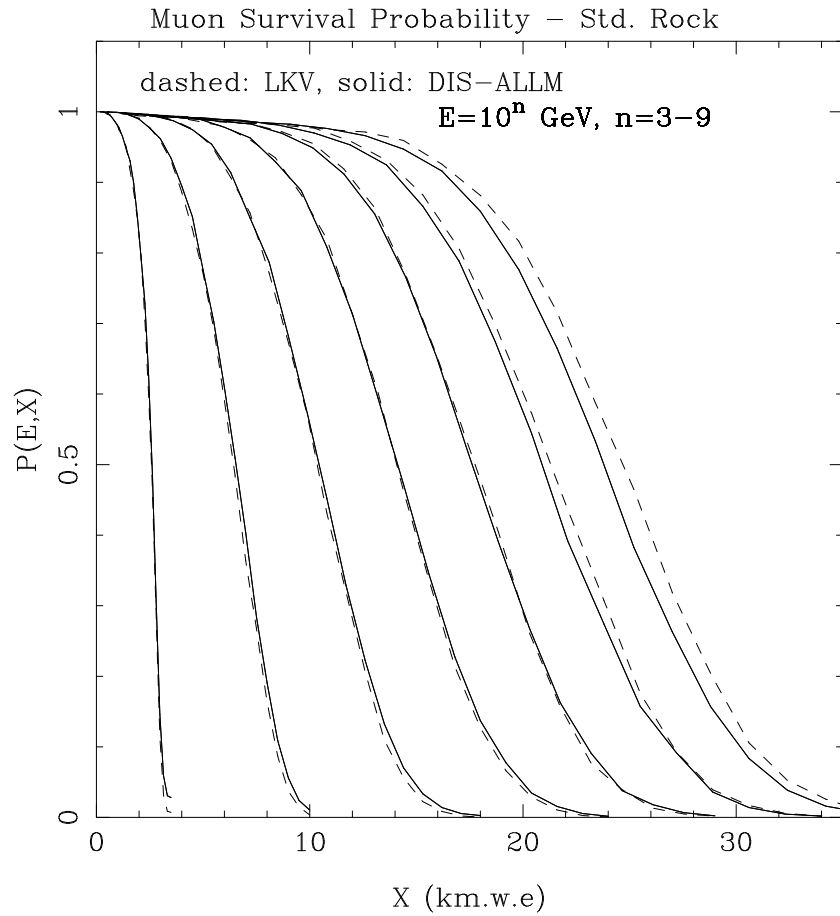


FIG. 4. Muon survival probabilities in rock using BB differential cross section for the photonuclear term (dashed) and the ALLM differential cross section (solid).

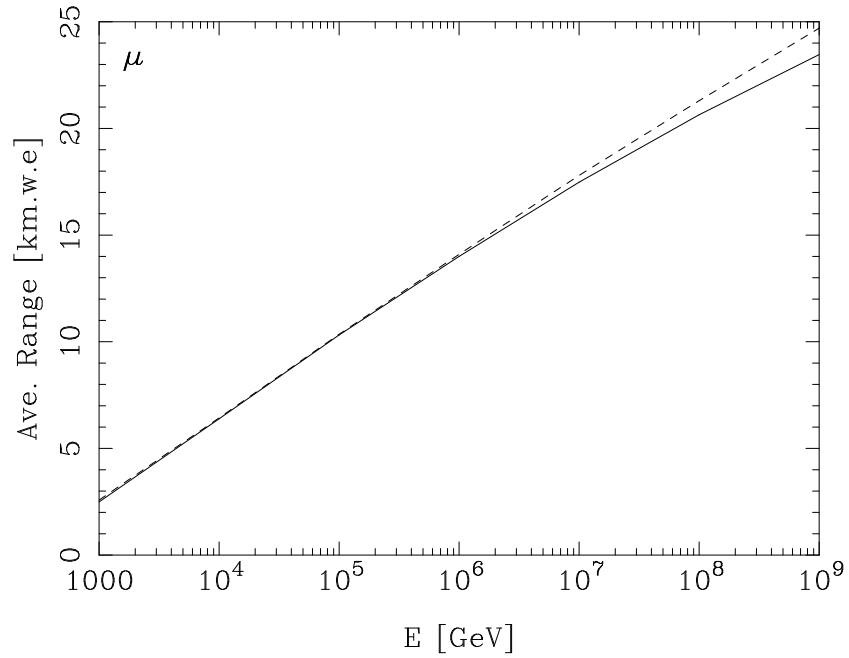


FIG. 5. Average muon range in standard rock (km.w.e. depth), for incident muon energy E , final muon energy $E_f \geq 1$ GeV, using the standard LKV treatment of energy loss, including the BB differential cross section (dashed) and substituting the ALLM photonuclear calculation (solid).

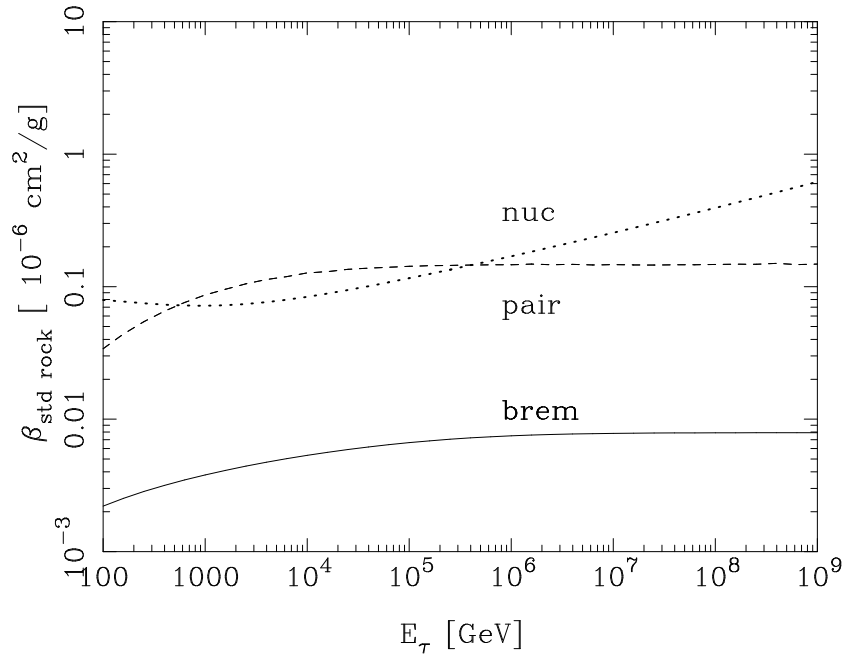


FIG. 6. The β value for tau in standard rock ($A = 22$), including bremsstrahlung (solid line), pair production (dashed) and photonuclear (ALLM) (dotted) interactions.

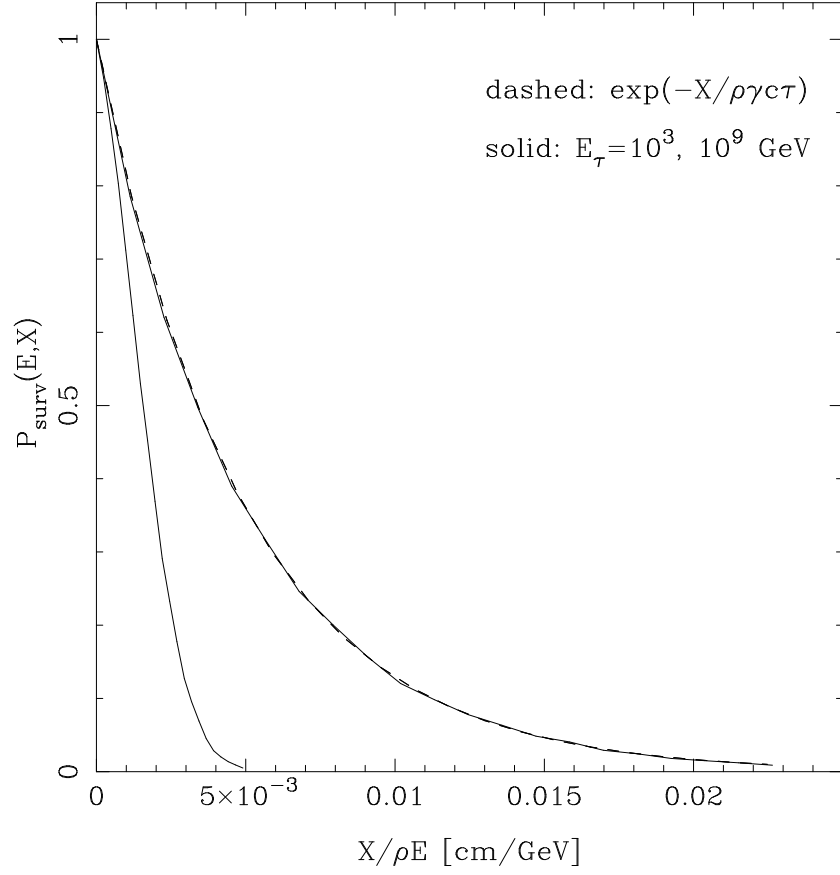


FIG. 7. Decay distribution(dashed line) and survival probability curve for incoming tau energy $E = 10^3$ GeV (upper solid line) and $E = 10^9$ GeV (lower solid line) in water ($\rho = 1$ g/cm³).

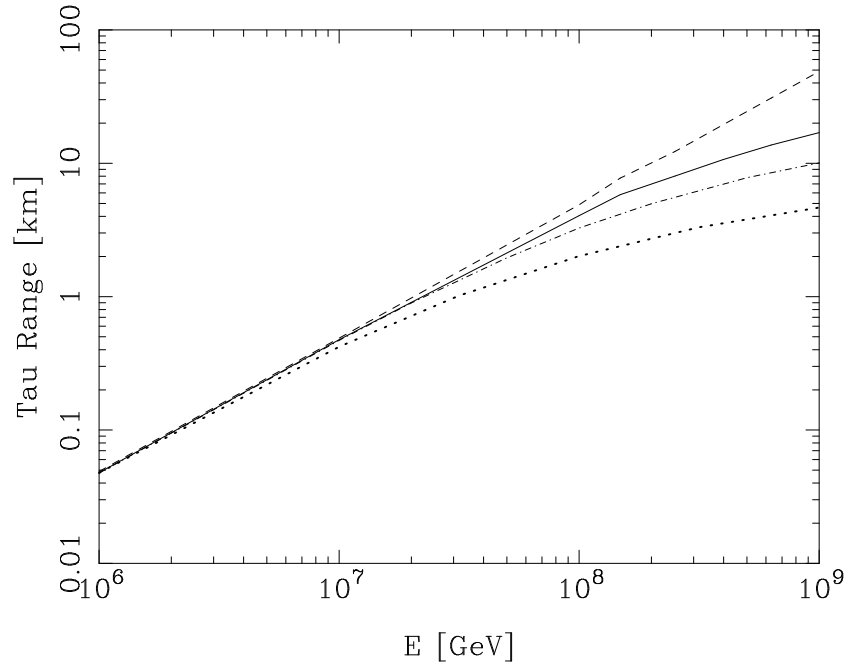


FIG. 8. Tau decay length (dashed line) and the average tau range in water (solid line), in rock (dot-dashed line) and in iron (dotted line), for incident tau energy E , final tau energy larger than $E_{min} = 50$ GeV including electromagnetic energy loss.